

Performance of Indoor VLC System Under Random Placement of LEDs With Nonimaging and Imaging Receiver

Anand Singh ¹, Graduate Student Member, IEEE, Anand Srivastava, Vivek Ashok Bohara ², Senior Member, IEEE, and Anand Kumar Jagadeesan

Abstract—This article analyzes the performance of multiple-input-multiple-output indoor visible light communication (VLC) system by randomly deploying the light-emitting-diodes (LEDs) using Matern hardcore point process (MHCP). Furthermore, photodetectors (PDs) with two different field of view (FOVs) have been utilized for an imaging as well as nonimaging receiver structures. It is a widely known fact that in a conventional VLC system, signal-to-noise ratio (SNR) profile inside the room varies with respect to the LED placement and the PDs position. Consequently, the proposed work attempts to achieve uniform SNR across the room, by utilizing MHCP based LED placement at the transmitter, and a nonimaging receiver with four PDs using 1-FOV, 2-FOV, and imaging receiver configurations. Simulation results show that random deployment of LED using MHCP configuration results in a more uniform SNR profile inside the room as compared to regular LED deployment schemes. Furthermore, three different power allocation schemes for LEDs namely equal power, distance-based power, and an optimal power allocation are proposed. For the different power allocation schemes, the average SNR and the variance of the received optical power (OP) inside the room are derived and compared. In addition, the closed-form expression for the bit-error-rate (BER) probability is derived for the proposed MHCP configuration using ON-OFF keying as a modulation scheme. Results show improvement in BER performance with the OP allocation in comparison to other power allocation schemes both for imaging and nonimaging receiver configuration.

Index Terms—Field-of-view (FOV), imaging receiver, multiple-input multiple-output (MIMO), nonimaging receiver, poisson point process (PPP), visible light communications.

I. INTRODUCTION

MOST of the current wireless networks utilize radio frequency based transmission. However, these networks are regularly confronted with the growing demand for higher data rates. For instance, viewing live stream high definition videos, online gaming, and cloud-based services are data-exhaustive

Manuscript received July 11, 2020; revised August 23, 2020; accepted August 24, 2020. (Corresponding author: Anand Singh.)

Anand Singh, Anand Srivastava, and Vivek Ashok Bohara are with the Department of Electronics and Communication Engineering, Indraprastha Institute of Information Technology Delhi, New Delhi 110020, India (e-mail: anandsi@iiitd.ac.in; anand@iiitd.ac.in; vivek.b@iiitd.ac.in).

Anand Kumar Jagadeesan is with the Cognizant, Chennai 600096, India (e-mail: anandkumar.jagadeesan@cognizant.com).

Digital Object Identifier 10.1109/JSYST.2020.3019823

activities that lead to a rapid depletion of data capacity [1]. Furthermore, such demand is more severe in indoor communication where the maximum data usage occurs. Visible light communication (VLC) is an optical wireless communication technology that can be used to fulfill the high capacity demand in an indoor scenario. In VLC, light-emitting diodes (LEDs) are used as transmitters, while photodetectors (PDs) are used as a receiver. The VLC system operates on intensity modulation direct detection (IM/DD) principle, where the information signal is modulated in terms of light intensity, and at the receiver, these intensity modulations are detected and converted into an electrical signal [2]. LEDs have modulation bandwidth up to 20 MHz, which can support very high data rate communications [3]. License-free deployment and nearly universal availability of LEDs make it an attractive and inexpensive choice for service providers.

The illumination in most indoor scenarios is provided by multiple LEDs located at specified intervals on the ceiling. As a consequence, at most locations within a room, light can be received from more than one source. When these luminaires are used as data transmitters, they can be configured in many ways. The simplest is to transmit the same signal from each luminaire. This potentially provides the best coverage but at the cost of diminished overall capacity. Alternatively, a cellular system can be constructed where each luminaire transmits data destined for the nearest receiver [4], [5]. The above-mentioned approach can be extended wherein the transmitters can be used in a multiple-input multiple-output (MIMO) configuration [6]. In MIMO configuration, the receiver must be able to separate signals from different sources. It has been shown in [7] that receiver with different field-of-view (FOV) can be used to separate the channel gains. This article further builds on the work in [7] and investigates the performance of random deployment of LEDs using the Matern hardcore point process (MHCP) by employing PDs with two different FOVs (2-FOV receivers) and the PDs with the same FOV (1-FOV receiver) referred as nonimaging receivers. The above-mentioned results have also been compared with imaging receiver configuration. Moreover, this article also compares the signal-to-noise ratio (SNR) performance at the receiver for the fixed geometry, i.e., circular geometry and the random geometry configurations that utilize the binomial point process (BPP) for LED placements.

A. Related Works

In indoor VLC system LEDs deployment plays an essential role, as the received optical power distribution (ROPD) varies with respect to the placement of LEDs and the location of the user inside the room. Consequently, ROPD can be improved by optimizing the placement of LEDs inside the room. Lei *et al.* [8] proposed an approach to obtain optimum spacing between LEDs in square geometry configuration and maximum radius of circle in case of circular geometry configuration to achieve uniform SNR across the room. Furthermore, to find the optimum location of the LEDs, a numerical optimization based local search algorithm is employed. The solution is obtained by an iterative process and remains suboptimal if the time bound expires. In [9], the relationship between the placement of LEDs and ROPD is studied, and a method is proposed to deploy the LED in a plane to improve the SNR at the receiver. In [10], an optimum placement of LEDs arrays is investigated for indoor VLC subject to maximization of average area spectral efficiency. Design parameters of the LED array such as the distance between two neighboring LEDs and the precise location of the LED arrays on the ceiling are obtained by solving the optimization problem. Due to the complexity of the optimization problem, a numerical optimization procedure is employed, and the maximization is carried out by using algorithms from MATLAB optimization toolbox. In [11], an ab initio design of a LED array for achieving uniform illumination is presented. Specifically, an optimization technique based on evolutionary programming has been developed to facilitate the search for an optimal array in the hyperspace formed by a number of LEDs and spacing among them. Singh *et al.* [12] analyze the performance of an indoor VLC system with randomly deployed LEDs and compared with existing random geometries like BPP and fixed geometries such as circular and square.

As evident from above, most of the conventional literature has focused on nonimaging receiver structure or investigated the placement of LEDs with regular geometry and equal power (EP) allocation to the individual LED sources. While uniform illuminance is desirable, optimal power (OP) consumption is an essential factor in the deployment of the LEDs. To address this issue, recent literature has focused on power allocation, along with flexibility in the LED source geometry to achieve uniform irradiance. In [13], hyperheuristics evolutionary algorithm is proposed to optimize the LED resources within an indoor room. Niaz *et al.* [14] proposed an optimized LED deployment technique to provide a better ROPD across the room while keeping the power consumption to minimum. In particular, the particle swarm optimization has been applied to minimize the overall outage area of an indoor VLC system. It is found that circular placement is the best among other fixed placement schemes such as the rectangular LED placement and circle-square placement. In [15], a network planning tool is provided to maximize the average rate achieved by the users in a room by optimizing the LED footprint. The proposed tool also takes into account the signaling needed to accomplish the handover task. In this regard, it is shown that several parameters influence system performance starting from the download data rate, the mobility of the user

in the room as well as the handover time. In [16], a genetic algorithm is proposed to optimize the refraction indices of the concentrators on receivers to achieve a uniform distribution of the received power, without decreasing the illuminance quality. Simulation results show that the proposed method can effectively reduce the ratio of power deviation from peak from 88% to 52%, with respect to the transmitted power.

B. Contribution

Motivated by these earlier works, in this article, we utilize MHCP to propose a random placement of LEDs in an indoor scenario to achieve uniform SNR and improved bit-error-rate (BER) performance at the receiver. It has been shown that MHCP is a desirable and more appropriate approach for LED placement.

The main contributions of this article are summarized as follows.

- 1) We propose a random placement scheme of LEDs using MHCP, which results in more uniform SNR throughout the room. The performance of the proposed scheme has been evaluated under two types of receiver structure with four PDs using 1-FOV and 2-FOV. Both nonimaging and imaging receiver configurations are considered in the analysis.
- 2) An optimal and distance-based power (DBP) allocation scheme is proposed to distribute the power across each LED. The proposed power allocation schemes have shown improved performance with respect to conventional EP allocation scheme.
- 3) The closed-form expression of BER for the MHCP based LED placement scheme for both optimal and DBP allocation with multiple PDs using 1-FOV and 2-FOV configurations has been derived.
- 4) Furthermore, the performance of imaging and nonimaging receiver for different power allocation schemes has been shown by plotting the cumulative distribution function (CDF) of the received power.

The rest of this article is organized as follows. In Section II, the system model for the proposed MHCP LED deployment and the receiver structure is described. In Section III, the optimal and DBP allocation schemes for the LEDs are explained. Closed-form expression of BER for the proposed system is derived in Section IV. The analytical and simulation results have been discussed in Section V. Finally, Section VI concludes this article.

Notations: The vector and the matrix are denoted as **seriesx** and **seriesX**, respectively. **seriesx^T** and **seriesX^T** denote the transpose of vector **seriesx** and matrix **seriesX**. The vectorization of matrix **X** is denoted as **X(:)**. The element corresponding to *i*th row and *j*th column of a matrix **seriesX** is represented as X_{ij} . The expectation and the variance of the random variable are denoted as E and Var , respectively. The set of positive real numbers is denoted by \mathbb{R}_+^N .

II. SYSTEM MODEL

We have considered a standard room size of 5 m × 5 m × 3 m. The 16 transmitting LEDs are placed in a random manner using the MHCP process, is shown in Fig. 1. The receiver

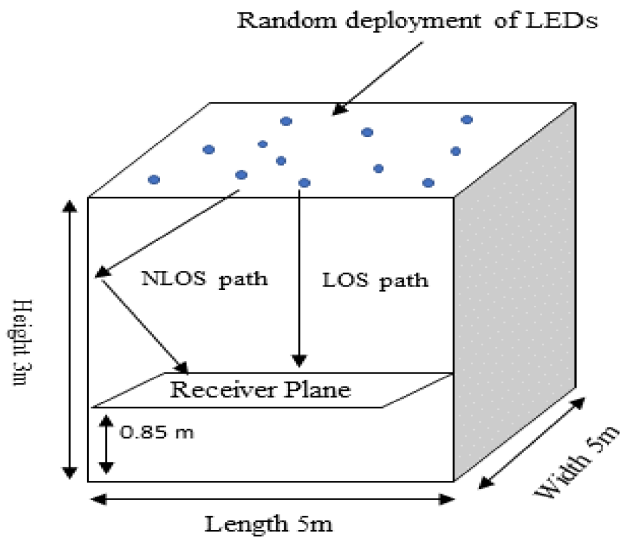


Fig. 1. System model.

structure consists of four PDs lying in a plane parallel to the LED array plane. We have used two types of receiver structures, namely nonimaging and imaging receiver structure. A nonimaging receiver structure consists of four discrete PDs arranged in a square panel with different FOVs. While an imaging receiver structure is modeled as an array of PDs with an imaging lens and a filter.

The following sections discuss about the LED placement strategy using MHCP as well as different receiver configurations.

A. Random Placement of LEDs

A point process is a collection of points randomly located on the space such as a real line, or a Cartesian plane. These point processes are frequently used in a telecommunication network for planning the location of base stations (BS) in a given area. MHCP is the clustered point process where, the points are forbidden to be closer than a certain minimum distance. In general, they are used in the planning of BS location, modeling of blockages, and interference calculation in wireless networks [17]. One way to achieve such a minimum distance between points is to start with a point process that has no such restriction and then remove points that violate the above-mentioned condition. Fig. 2 shows the realization of 16 LEDs in MHCP configuration.

In this article, we have used the MHCP process to distribute the LEDs in a plane with intensity λ , which is defined by the number of LEDs to be deployed. The hardcore distance δ can be treated as a contact distribution as it specifies the probability that two points within δ distance of each other are retained, which is same as saying that two points are separated by distance δ in MHCP [18].

To determine the intensity of the MHCP process, we first condition on a point having a given mark t . This point is retained with probability of $\exp(-t\pi\delta^2)$. Since $t\lambda_b$ is the density of points with marks smaller than t , the intensity of the resulting

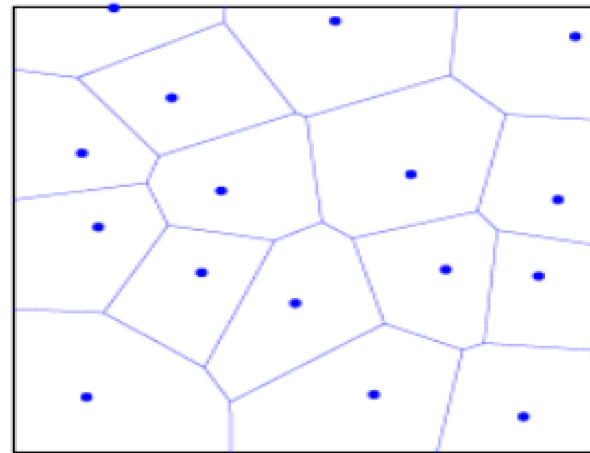


Fig. 2. Realization of MHCP with 16 LEDs.

process is given as [19]

$$\lambda = \lambda_b \int_0^1 \exp(-t\lambda_b\pi\delta^2) dt = \frac{1 - \exp(-\lambda_b\pi\delta^2)}{\pi\delta^2}. \quad (1)$$

B. Receiver Structure

1) *Nonimaging Receiver*: In this section, the nonimaging receiver with 1-FOV and 2-FOV configuration is discussed. For a good VLC MIMO receiver for indoor optical wireless applications must have these two characteristics.

- 1) The receiver should have a large FOV so that it has a line of sight (LoS) from as many numbers LED transmitters as possible.
- 2) It should provide good diversity so that the signals from different transmitters can be separated [7].

In the 2-FOV receiver, the PDs with large FOV ensure that the receiver has a large overall FOV so that it has LOS to all the LED luminaires from all the possible receiver positions. The PDs having narrow FOV is used to reduce the similarity between the channel gain in each column of the channel matrix because, for most receiver positions, some luminaires are outside of the FOV of some PDs and within the FOV of others. Thus, even when the distance between the PDs is small, the channel matrix is well conditioned [7]. In this article, we have used a combination of large FOV 60° and small FOV 30° receiver, as shown in Fig. 3. The reason behind using FOV combination of 60° and 30° is because, this combination provides a better-conditioned channel matrix than any other FOV combination, which will help the receiver in signal extraction [7]. Fig. 3(a) shows the nonimaging receiver configuration with four PDs having the same FOV of 60° and Fig. 3(b) shows the nonimaging receiver configuration with four PDs having different FOV of 60° and 30° , respectively.

2) *Imaging Receiver*: In this section, the imaging receiver is discussed. The imaging receiver is a collection of PDs arranged in a rectangular array. Fig. 4 shows the schematic of the imaging receiver in a room with the concentrator (imaging lens) followed by a PD array and an amplifier [20]. The PD array collects transmitting data in the form of light from all parts of the room, which

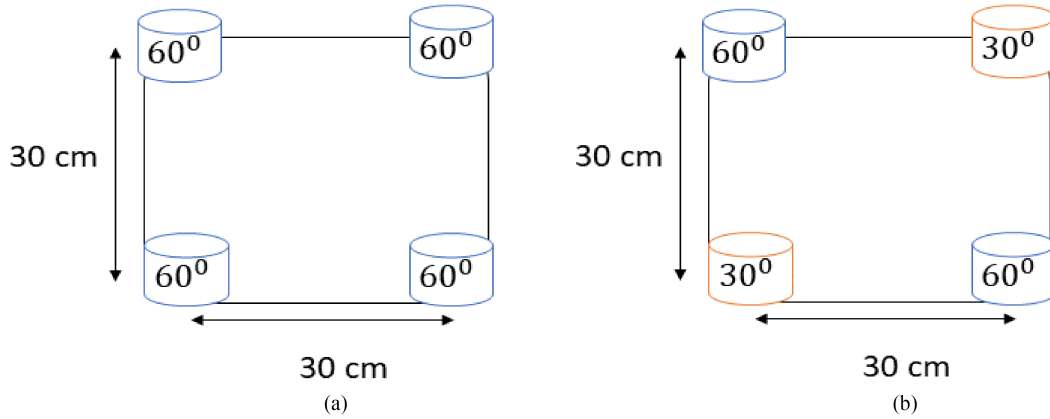


Fig. 3. Nonimaging receiver structure with four PDs in 1-FOV and 2-FOV configuration. (a) 1-FOV. (b) 2-FOV.

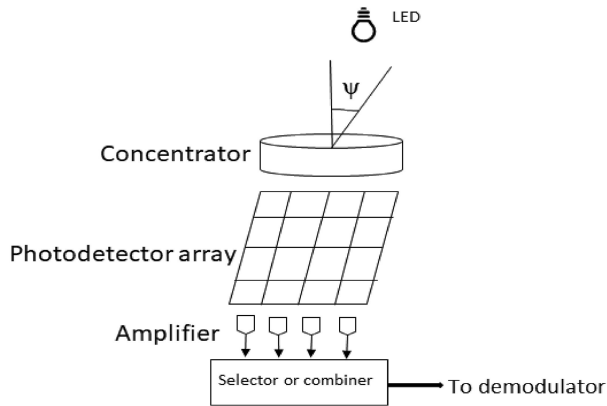


Fig. 4. Imaging receiver.

creates an equivalent photo-current, which is further converted in the useful received signal. Light transmitting from the source LEDs to the receiver, and each LED array is imaged onto a PD array, where images may strike any pixels or group of pixels on the array. Each pixel on the PD array acts as a receiver channel, which calculates the value of the channel matrix between each transmitting LED and the receiver. This channel matrix helps in distinguishing the signal received from different LEDs.

III. LED POWER ALLOCATION SCHEMES

In this article, we have proposed three LED power allocation strategy for MHCP in order to maximize the received power at the receiver plane.

A. EP Allocation

In the equal LED power allocation strategy, the total LED transmit power is equally divided among N randomly placed LEDs. The total LED transmit power can be expressed as follows:

$$P_T = \sum_{i=1}^N P_{t_i}. \quad (2)$$

where P_{t_i} is the allocated power to the i th LED.

B. DBP Allocation

In the proposed MHCP configuration LEDs are placed at the arbitrary locations, so the transmitted power will be conditioned on the distance of the LED from the center of the LEDs array. In this power allocation strategy, the total power is distributed among all the LEDs. The power distribution is the function of the distance of the i th LED from the center of the array. Hence, the power allocated to i th LED is expressed as follows:

$$P_{t_i} = \frac{d_i^\alpha P_T}{\sum_{i=1}^N d_i^\alpha}, \quad (3)$$

where d_i is the distance of i th LED from the center of the array, P is total transmit power, and α is the path exponent. The received power at PDs and can be written in terms of transmitting power as follows:

$$P_{r_j} = \sum_{i=1}^N H_{ij} P_{t_i}. \quad (4)$$

H_{ij} is the VLC channel gain between i th LED and j th PD and can be expressed as [21] [22]

$$H_{ij} = \frac{(m+1)\cos^m(\phi)A\cos(\theta)}{2\pi d_{ij}^2}. \quad (5)$$

where ϕ is the angle of incidence of light on the surface and m is the order of Lambertian emission, A is the detector physical area, and θ is the angle of incidence with respect to the receiver axis, d_{ij} is the distance between the i th LED and the j th PD. The exponent α is calculated in order to maximize the SNR at the receiver. For a MHCP, the expected SNR at the j th PD can be written as follows:

$$\text{SNR}_j = \text{E} \left[\frac{P_{r_j}}{\sigma_j^2} \right]. \quad (6)$$

where E is expectation operator and σ_j^2 is the noise variance at the j th PD. To find the optimum value of α iterative search algorithm is used [23]. To maximize the SNR_j in (6), the value of α is found to be 3.1 for the proposed MHCP with 16 LEDs.

C. Optimum Power Allocation

In order to maintain uniform SNR across the room, it is essential that the mean SNR at the receiver is above a given threshold and the variance of the SNR should be small. The variance of the received power P_{r_j} at j th location in the room is considered a cost function which should be minimized in order to get uniform SNR at the receiver plane and is expressed as follows:

$$\min_{P_{t_i}} \left[\mathbb{E} \left[P_{r_j}^2 \right] - \left(\mathbb{E} [P_{r_j}] \right)^2 \right] \quad (7)$$

subject to following constraints.

- 1) The sum of each LED power (P_T) watts should be constant

$$\begin{aligned} \sum_{i=1}^N P_{t_i} &= P_T, \\ \Rightarrow 1_N \mathbf{x} &= P_T. \end{aligned} \quad (8)$$

where, 1_N is a N dimensional unit vector and $\mathbf{x} = [P_{t_1}, \dots, P_{t_N}]^T$ is N dimensional column vector of decision variables.

- 2) The power of each source LED is always non-negative.

$$P_{t_i} \geq 0 \quad \forall i = 1, \dots, N \quad (9)$$

$$\Rightarrow \mathbf{G} \mathbf{x} \geq 0. \quad (10)$$

where $\mathbf{G} = \text{diag}(1, \dots, 1)$.

The first term in (7) is a second order mean and can be calculated by taking second order expectation of the received power P_{r_j}

$$\begin{aligned} \mathbb{E} \left[(P_{r_j})^2 \right] &= \mathbb{E} \left[\left(\sum_{i=1}^N H_{ij} P_{t_i} \right)^2 \right] \\ &= \mathbb{E} \left[\sum_{i=1}^N H_{ij}^2 P_{t_i}^2 + 2 \sum_{i=1}^N \sum_{q=i+1}^N H_{ij} H_{qj} P_{t_i} P_{t_q} \right] \\ &= \frac{\sum_{j=1}^K \sum_{i=1}^N H_{ij}^2 P_{t_i}^2}{K} \\ &\quad + \frac{\sum_{j=1}^K 2 \sum_{i=1}^N \sum_{q=i+1}^N H_{ij} H_{qj} P_{t_i} P_{t_q}}{K} \\ &= \frac{\sum_{i=1}^N \mu_{ii} P_{t_i}^2 + 2 \sum_{i=1}^N \sum_{q=i+1}^N \mu_{iq} P_{t_i} P_{t_q}}{K}, \end{aligned} \quad (11)$$

where $\mu_{iq} = \sum_{j=1}^K H_{ij} H_{qj}$ and K is the total number of PD. The second term in (7) is a square of first order mean of received power P_{r_j} and can be expressed as follows:

$$\begin{aligned} \left(\mathbb{E} [P_{r_j}] \right)^2 &= \left(\frac{\sum_{j=1}^K P_{r_j}}{K} \right)^2 = \left(\frac{\sum_{j=1}^K \sum_{i=1}^N H_{ij} P_{t_i}}{K} \right)^2 \\ &= \left(\frac{\sum_{i=1}^N \gamma_i P_{t_i}}{K} \right)^2 \end{aligned} \quad (12)$$

where $\gamma_i = \sum_{j=1}^K H_{ij}$

$$\left(\mathbb{E} [P_{r_j}] \right)^2 = \frac{\sum_{i=1}^N \gamma_i^2 P_{t_i}^2 + 2 \sum_{i=1}^N \sum_{p=i+1}^N \gamma_i \gamma_p P_{t_i} P_{t_p}}{K^2}. \quad (13)$$

Substituting (11) and (13) in (7), variance can be obtained as follows:

$$\begin{aligned} \text{Var}(P_{r_j}) &= \mathbb{E} \left[(P_{r_j})^2 \right] - \left(\mathbb{E} [P_{r_j}] \right)^2 \\ &= \frac{\sum_{i=1}^N \mu_{ii} P_{t_i}^2 + 2 \sum_{i=1}^N \sum_{q=i+1}^N \mu_{iq} P_{t_i} P_{t_q}}{K} \\ &\quad - \frac{\sum_{i=1}^N \gamma_i^2 P_{t_i}^2 + 2 \sum_{i=1}^N \sum_{p=i+1}^N \gamma_i \gamma_p P_{t_i} P_{t_p}}{K^2} \\ &= \sum_{i=1}^N \left(\frac{\mu_{ii}}{K} - \frac{\gamma_i^2}{K^2} \right) P_{t_i}^2 \\ &\quad + 2 \sum_{i=1}^N \sum_{q=i+1}^N \left(\frac{\mu_{iq}}{K} - \frac{\gamma_i \gamma_q}{K^2} \right) P_{t_i} P_{t_q}. \end{aligned} \quad (14)$$

By substituting the value of μ_{ii} , μ_{iq} , γ_i , and γ_p , respectively, and taking the factor $\frac{1}{2}$ common from both the terms in (14) the variance can be expressed as follows:

$$\begin{aligned} &= \frac{1}{2} \left[\sum_{i=1}^N \left\{ \frac{2 \sum_{j=1}^K H_{ij}^2}{K} - \frac{2 \left(\sum_{j=1}^K H_{ij} \right)^2}{K^2} \right\} P_{t_i}^2 \right. \\ &\quad \left. + 2 \sum_{u=1}^N \sum_{v=i+1}^N \left\{ \frac{2 \sum_{j=1}^K H_{uj} H_{vj}}{K} \right. \right. \\ &\quad \left. \left. - \frac{2 \left(\sum_{j=1}^K H_{uj} \right) \left(\sum_{j=1}^K H_{vj} \right)}{K^2} \right\} P_{t_u} P_{t_v} \right] \end{aligned} \quad (15)$$

$$= \frac{1}{2} \left[P_{t_1}, \dots, P_{t_N} \right] \begin{bmatrix} \beta_{11} & \dots & \beta_{1N} \\ \dots & \dots & \dots \\ \beta_{N1} & \dots & \beta_{NN} \end{bmatrix} \begin{bmatrix} P_{t_1} \\ \dots \\ P_{t_N} \end{bmatrix}. \quad (16)$$

Therefore, the proposed optimization problem can be expressed in matrix form as follows:

$$\min_{\mathbf{x}} \frac{1}{2} \mathbf{x}^T \mathbf{P} \mathbf{x} \quad (17)$$

subject to

$$1_N \mathbf{x} = P_T \quad (18)$$

$$\mathbf{G} \mathbf{x} \geq 0. \quad (19)$$

where the matrix \mathbf{P} using (15) is given by

$$\mathbf{P} = \begin{bmatrix} \beta_{11} & \dots & \beta_{1N} \\ \dots & \dots & \dots \\ \beta_{N1} & \dots & \beta_{NN} \end{bmatrix} \quad (20)$$

and elements β_{uv} are

$$\beta_{uv} = \begin{cases} \frac{2 \sum_{p=1}^K H_{up}^2}{K} - \frac{2(\sum_{p=1}^K H_{up})^2}{K^2}, & u = v \\ \frac{2 \sum_{p=1}^K H_{up} H_{vp}}{K} - \frac{2(\sum_{p=1}^K H_{up})(\sum_{p=1}^K H_{vp})}{K^2}, & u \neq v. \end{cases} \quad (21)$$

Here, (18) and (19) corresponds to the two constraint that we stated during problem formulation (7).

IV. BER PERFORMANCE

We have assumed ON-OFF (OOK) keying modulation in the VLC link for deriving the BER expression as this is one of the standard modulation scheme defined in the VLC standard (IEEE 802.15.7) [24]. The optical signal transmitted by the i th LED of the VLC is given by

$$s_i(t) = P_{t_i}[1 + M_I x_i(t)] \quad (22)$$

where P_{t_i} is the power allotted to the i th source LED, x_i is the respective information modulated as OOK signal, and M_I is the modulating index [25]. After the signal is received by a PD, the dc component of the transmitting signal is filtered out and the final received signal at j th PD is given by

$$y_j = \mathcal{R}P_{r_j} + n_j \quad (23)$$

where \mathcal{R} is photodiode responsivity, n_j is additive white Gaussian noise (AWGN) with $n_j = \mathcal{N}(0, \sigma_j^2)$ and P_{r_j} is expressed as follows:

$$P_{r_j} = \sum_{i=1}^N H_{ij} P_{t_i} M_I x_i. \quad (24)$$

The noise σ_j^2 at j th the PD is the total noise power comprising of shot noise power (σ_{shot}^2) and thermal noise power ($\sigma_{\text{thermal}}^2$) which can be expressed as

$$\sigma_j^2 = \sigma_{\text{shot}}^2 + \sigma_{\text{thermal}}^2 \quad (25)$$

where

$$\sigma_{\text{shot}}^2 = 2e\mathcal{R}P_{r_j}B_s + 2eI_{\text{bg}}I_2B_s \quad (26)$$

and

$$\sigma_{\text{thermal}}^2 = \frac{8\pi k T_k}{G} \eta A_r I_2 B_s^2 + \frac{16\pi^2 k T_k \Gamma}{g_m} \eta^2 A_r^2 I_3 B_s^3. \quad (27)$$

where e is the electron charge, P_{r_j} is the received optical power at j th PD, A_r is the PD effective receiver area, B_s is the system bandwidth, I_{bg} is the received background noise current, k is Boltzmann's constant, T_k is the absolute temperature, G is the open loop voltage gain, η is the fixed capacitance of PD per unit area, Γ is the field effect transistor (FET) channel noise factor, g_m is the FET transconductance, I_2 is the noise bandwidth factor for background noise, and I_3 is the noise bandwidth factor.

A. BER for EP Allocation

For EP allocation, the SNR at the receiver using minimum mean square error (MMSE) equalizer at the output of the PD is

expressed as [26]:

$$\text{SNR}_{\text{EP}} = \frac{(\mathcal{R}P_T)^2}{\sigma_j^2 \left[\left(\mathbf{H}^T \mathbf{H} + \frac{\sigma_j^2 \mathbf{I}}{(\mathcal{R}P_T)^2} \right)^{-1} \right]}, \quad (28)$$

where \mathbf{H} is the channel matrix and can be calculated using (5), and \mathbf{I} is the identity matrix. BER for VLC with OOK under AWGN can be defined as [27]:

$$\begin{aligned} \text{BER}_{\text{EP}} &= Q\left(\sqrt{\text{SNR}_{\text{EP}}}\right) \\ &= Q\left(\sqrt{\frac{(\mathcal{R}P_T)^2}{\sigma_j^2 \left[\left(\mathbf{H}^T \mathbf{H} + \frac{\sigma_j^2 \mathbf{I}}{(\mathcal{R}P_T)^2} \right)^{-1} \right]}}\right). \end{aligned} \quad (29)$$

BER calculation is done using (29) for both 1-FOV and 2-FOV configuration, where only the channel matrix \mathbf{H} value will change as per the configuration of the receiver.

B. BER for DBP Allocation

For DBP allocation, the SNR at the receiver can be written as follows:

$$\text{SNR}_{\text{DBP}} = \sum_{j=1}^K \left[\frac{\left(\mathcal{R} \sum_{i=1}^N H_{ij} P_{t_i} \right)^2}{\sigma_j^2} \right] \quad (30)$$

where P_{t_i} will be calculated according to DBP allocation strategy, which satisfies (6). BER for OOK with DBP allocation can be expressed as

$$\begin{aligned} \text{BER}_{\text{DBP}} &= Q\left(\sqrt{\text{SNR}_{\text{DBP}}}\right) \\ &= Q\left(\sqrt{\sum_{j=1}^K \left[\frac{\left(\mathcal{R} \sum_{i=1}^N H_{ij} P_{t_i} \right)^2}{\sigma_j^2} \right]}\right). \end{aligned} \quad (31)$$

The \mathbf{H} matrix calculation will remain same for both equal and DBP allocation schemes.

C. BER for OP Allocation

For the OP allocation, the transmit power to the i th LED will be allocated using optimization problem formulated in (7), which will depend on the MHCP process. The SNR at the j th PD for OP allocation can be written as follows:

$$\text{SNR}_j = E \left[\frac{\left(\mathcal{R} \sum_{i=1}^N H_{ij} P_{t_i} \right)^2}{\sigma_j^2} \right] \quad (32)$$

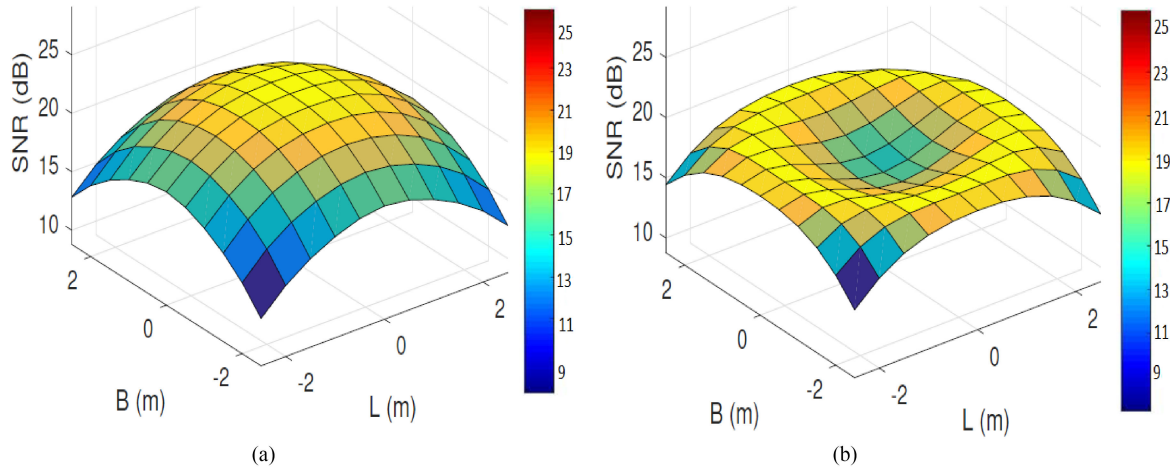


Fig. 5. Received SNR distribution for 1-FOV and 2-FOV receiver with EP allocation. (a) 1-FOV. (b) 2-FOV.

TABLE I
SYSTEM MODEL PARAMETERS

Parameter	Value
Room size ($W \times L \times H$)	5 m \times 5 m \times 3 m
Number of LEDs	16
Total LED transmitted power	2 Watt
Center luminous intensity of LED	0.73 cd
Wall reflection ρ	0.8
LED irradiance angle	60°
Receiver plane above the floor	0.85 m
Receiver elevation	90°
Receiver active area	1 cm ²
Field-of-views (FOVs) of receiver	60°, 30°
Responsivity	0.5 $\frac{A}{W}$
Noise bandwidth factor I_2	0.562
Background current I_{bg}	100 μA

The SNR at the receiver for optimal allocation can be written as follows:

$$SNR_{OP} = \frac{\mathcal{R}^2 \sum_{j=1}^K \sum_{i=1}^N H_{ij}^2 P_{t_i}^2}{\sigma_j^2}. \quad (33)$$

Therefore, the BER expression with OOK for OP allocation can be expressed as follows:

$$\begin{aligned} BER_{OP} &= Q\left(\sqrt{SNR_{optimal}}\right) \\ &= Q\left(\sqrt{\frac{\mathcal{R}^2 \sum_{j=1}^K \sum_{i=1}^N H_{ij}^2 P_{t_i}^2}{\sigma_j^2}}\right). \end{aligned} \quad (34)$$

BER calculation for OP allocation with 1-FOV and 2-FOV can be computed using (34). It can not be further decomposed analytically due to summation included in the point process hence will be evaluated numerically.

V. RESULTS AND DISCUSSION

In this section, we present simulation and analytical results for the proposed system inside a standard room size of 5 m \times 5 m \times 3 m. The room consists of 16 LED transmitters

placed in a random geometry using MHCP and a receiver consist of four PDs in a square geometry with nonimaging (1-FOV and 2-FOV) and an imaging receiver. The system model parameters of the VLC transmitters and the receiver are provided in Table I. We have used colormap (jet) of the MATLAB, to show the corresponding data values with a specific color. Each row in colormap contains the red, green, and blue intensities for a specific color. The minimum and maximum obtained data value are shown with blue and red colors, respectively.

A. Received SNR Profile

In this section, the SNR distribution at the receiver for the proposed MHCP configuration with LED power allocation schemes under 1-FOV, and 2-FOV receiver structure with four PDs are shown using simulation results.

1) *EP Allocation*: Fig. 5 shows the SNR profile at the receiver for proposed MHCP geometry with $N = 16$ LEDs for 1-FOV and 2-FOV receiver with four PDs. The total power is equally distributed among LEDs. With the help of the received SNR profile from Fig. 5(a) and (b), it can be calculated that for EP allocation with 1-FOV receiver, the average SNR at the receiver is 13.50 dB whereas, for 2-FOV receiver, the average SNR at the receiver is 14.20 dB. Also 1-FOV receiver performance is poor because all of the elements in the channel matrix have very similar values, so the MMSE equalizer causes considerable noise enhancement. In a 2-FOV receiver, the combination of low and high FOV results in a more conditioned channel matrix than 1-FOV receiver, which results in improved channel gain at the receiver.

2) *DBP Allocation*: For the proposed MHCP geometry of LED deployment, the LEDs are located at an arbitrary location in the transmitting plane. In the DBP allocation strategy, the transmit power will also depend on the distance of the LED from the center of the MHCP array. The total power is distributed across $N = 16$ LEDs using (3), which maximizes the SNR at the receiver.

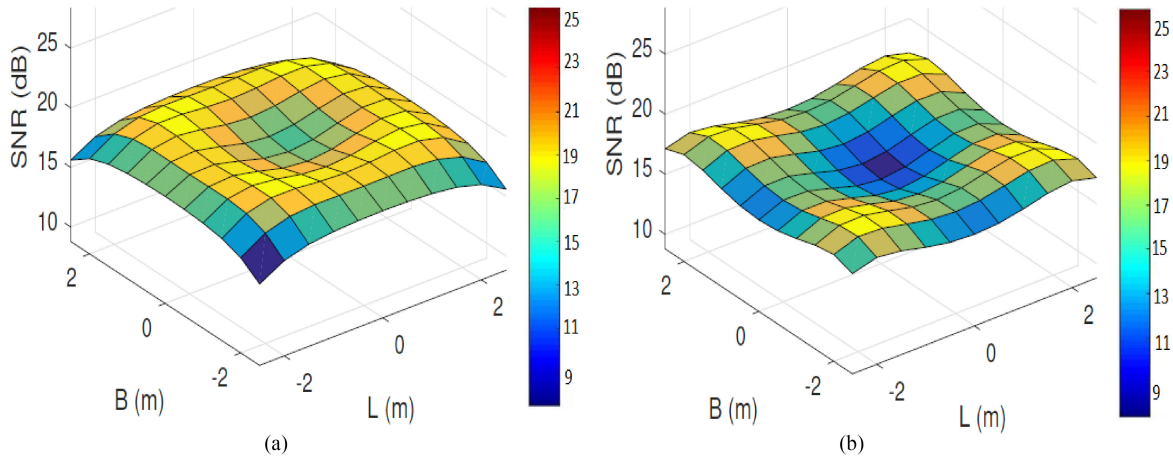


Fig. 6. Received SNR distribution for 1-FOV and 2-FOV receiver with DBP allocation. (a) 1-FOV. (b) 2-FOV.

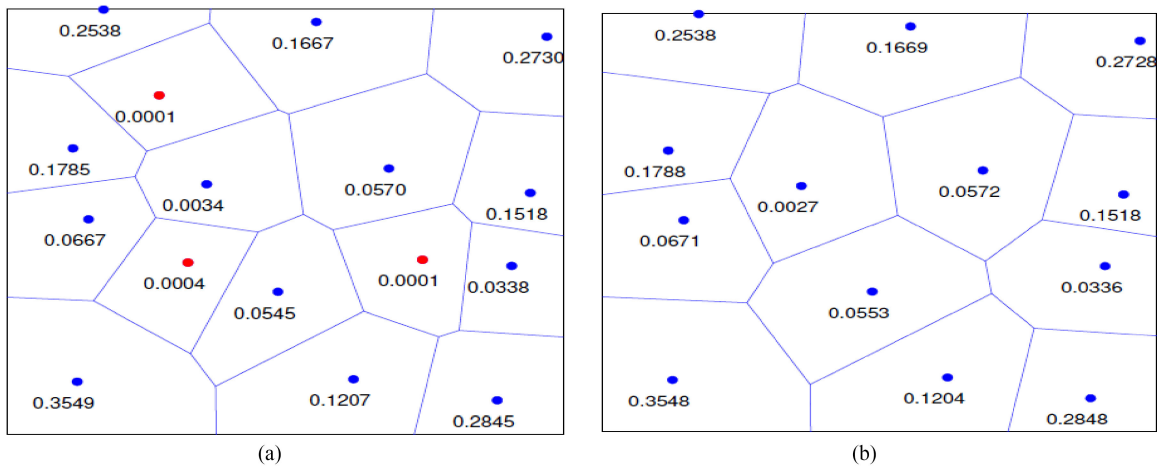


Fig. 7. Optimal distribution of total transmit power across source LEDs. (a) MHCP with 16 LEDs. (b) MHCP with 13 LEDs.

Fig. 6 shows the SNR profile at the receiver for proposed MHCP with $N = 16$ LEDs with 1-FOV and 2-FOV receiver configuration. For 1-FOV with DBP allocation, the average SNR is 17.34 dB, while with 2-FOV receiver, the average SNR is 18.26 dB, as shown in Fig. 6(a) and (b). The 2-FOV receiver structure performs better than the 1-FOV receiver.

3) *OP Allocation*: Fig. 7 shows the realization of LEDs using the MHCP with an OP allocation scheme. The total transmit power of P Watt is distributed among 16 LEDs by solving the proposed optimization problem in (17). It was observed that three LEDs which are marked as red in Fig. 7(a), have very less transmit power distributed compared to others, hence these three LEDs can be ignored in realization as shown in Fig. 7(b).

Fig. 8(a) and (b) compares the SNR profile at the receiver for 1-FOV and 2-FOV receiver with 16 LEDs in MHCP using OP allocation. It can be observed that for OP allocation with 16 LEDs, 2-FOV receiver performs better with an average SNR of 21.15 dB with respect to 1-FOV receiver, which has an average SNR of 18.85 dB. Furthermore, by removing three LEDs, which are transmitting negligible power as compared to other LEDs

and with OP allocation among 13 LEDs, it is observed that the SNR profile at the receiver is not affected. It is still comparable to the average SNR of 16 LEDs with low variance, as shown in Fig. 9(a) and (b).

It may be noted that illumination is considered as a primary functionality of the LEDs and is given priority over communication [28]. To calculate illumination for a VLC system, it is assumed that each LED has a Lambertian radiation pattern, with the Lambert index m , depending on the half-power angle of LED $\Phi_{\frac{1}{2}}$, $m = \frac{-1}{\log_2(\cos \Phi_{\frac{1}{2}})}$. The luminous intensity for LED transmitting power P_t in angle ϕ is given by

$$I(\phi) = \frac{P_t \cos^m \phi}{4\pi r^2} = I(0)\cos(\phi). \quad (35)$$

where $I(0) = \frac{P_t}{4\pi r^2}$, is the maximum intensity of the flux with angle $\phi = 0^\circ$. A horizontal illuminance E_{hor} , at a point (x,y) is given by

$$E_{\text{hor}} = \frac{I(0)\cos^{m+1}(\phi)}{d^2} \cdot \cos(\theta) \quad (36)$$

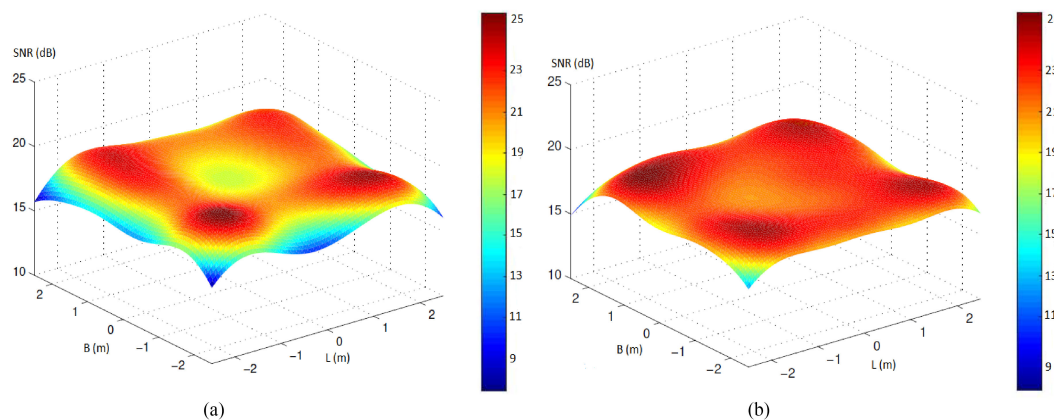


Fig. 8. Received SNR profile for 1-FOV and 2-FOV receiver with 16 LEDs in MHCP with OP allocation. (a) 1-FOV. (b) 2-FOV.

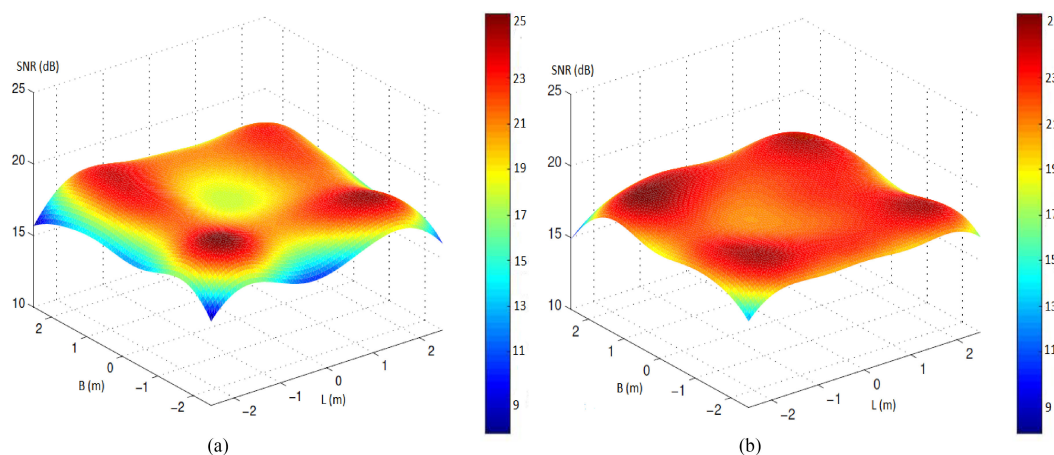


Fig. 9. Received SNR profile for 1-FOV and 2-FOV receiver with 13 LEDs in MHCP with OP allocation. (a) 1-FOV. (b) 2-FOV.

TABLE II
SNR PERFORMANCE OF LEDs IN CIRCULAR GEOMETRY

Parameter	Equal power (EP)		distance-based power (DBP)		Optimal power (OP)	
	1-FOV	2-FOV	1-FOV	2-FOV	1-FOV	2-FOV
Mean SNR	12.35 dB	14.50 dB	16.50 dB	17.85 dB	18.25 dB	19.20 dB
Variance of ROPD	2.75 dBm	2.20 dBm	2.13 dBm	1.65 dBm	0.982 dBm	0.650 dBm
Illumination	340-1300 lux	340-1300 lux	340-1350 lux	340-1350	360-1350 lux	360-1350 lux

TABLE III
SNR PERFORMANCE OF LEDs IN MHCP CONFIGURATION WITH NONIMAGING RECEIVER

Parameter	Equal power (EP)		distance-based power (DBP)		Optimal power (OP)	
	1-FOV	2-FOV	1-FOV	2-FOV	1-FOV	2-FOV
Mean SNR	13.50 dB	14.20 dB	17.34 dB	18.26 dB	18.85 dB	21.15 dB
Variance of ROPD	2.67 dBm	2.11 dBm	1.798 dBm	0.821 dBm	0.693 dBm	0.380 dBm
Illumination	330-1320 lux	330-1320 lux	350-1350 lux	350-1350	380-1400 lux	380-1400 lux

where d is the distance between the LED and the receiver surface. For the three-dimensional illumination profile generation, the room floor is divided into grids, and illumination for each grid using the (34) is calculated. The standard illuminance requirement for indoor room lighting for office work is 300–1500 lux standardized by the International Standard Organization (ISO), it is fulfilled by the proposed geometry [29]. Hence, from the

above-mentioned discussion, it can be inferred that the proposed work improves the system’s performance without compromising the illuminance.

The SNR performance for all three power allocation strategies for the proposed MHCP with 1-FOV and 2-FOV receiver structure is summarized in Table III. We have also compared the performance of MHCP geometry with circular geometry and

TABLE IV
SNR PERFORMANCE OF LEDs IN MHCP CONFIGURATION WITH IMAGING RECEIVER

Parameter	Equal power (EP)	Distance-based power (DBP)	Optimal power (OP)
Mean SNR	15.30 dB	19.22 dB	22.45 dB
Variance of ROPD	1.76 dBm	1.05 dBm	0.5. dBm
Illumination	330-1320 lux	350-1350 lux	380-1400 lux

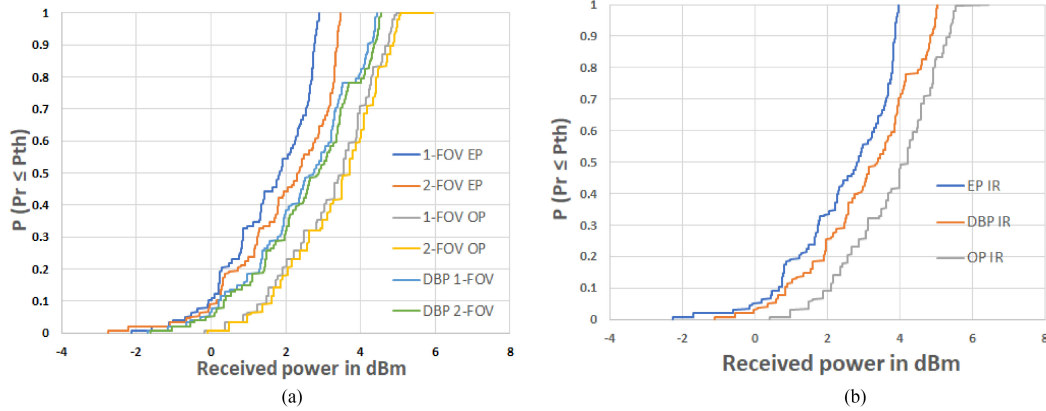


Fig. 10. CDF of received power in MHCP with EP, DBP, and OP allocation. (a) CDF of received power in MHCP with nonimaging receiver. (b) CDF of received power in MHCP with imaging receiver.

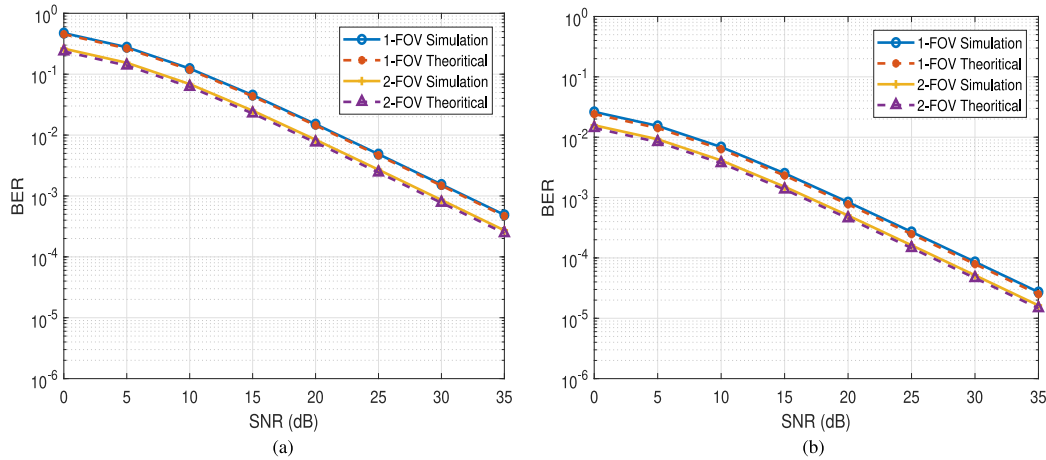


Fig. 11. BER performance of the MHCP with nonimaging 1-FOV and 2-FOV receiver. (a) BER performance with EP allocation. (b) BER performance with OP allocation.

MHCP performance with imaging receiver, as shown in Tables II and IV, respectively. The proposed MHCP based OP allocation in LEDs performs better than the circular geometry in EP and DBP allocation strategies for 1-FOV and 2-FOV nonimaging receiver.

MHCP with optimum power in imaging receiver performs even better, and it is due to the fact that in imaging receiver both LOS and non-LOS links reduce ambient light noise, receiver thermal noise, and multipath distortion, which results in improved SNR at the receiver [30]. To further elaborate the results obtained for MHCP in Tables III and IV, we have plotted the CDF of received optical power in MHCP configuration, as

shown in Fig. 10. It shows the probability that the received optical power P_r is less than or equal to the corresponding received optical power P_{th} in dBm [$P(P_r \leq P_{th})$] for different power allocation strategies. For instance, as shown in Fig. 10(a), at the probability of 0.5, the received optical power in EP allocation scheme with 1-FOV, and 2-FOV configuration is less than the 1.83 and 2.35 dBm, respectively. For the DBP allocation scheme at the probability of 0.5, the received optical power in 1-FOV, and 2-FOV configuration is less than the 2.75 and 3.10 dBm, respectively. For the OP allocation scheme at the probability of 0.5, the received optical power in 1-FOV, and 2-FOV configuration is less than the 3.25 and 3.80 dBm, respectively. Similarly,

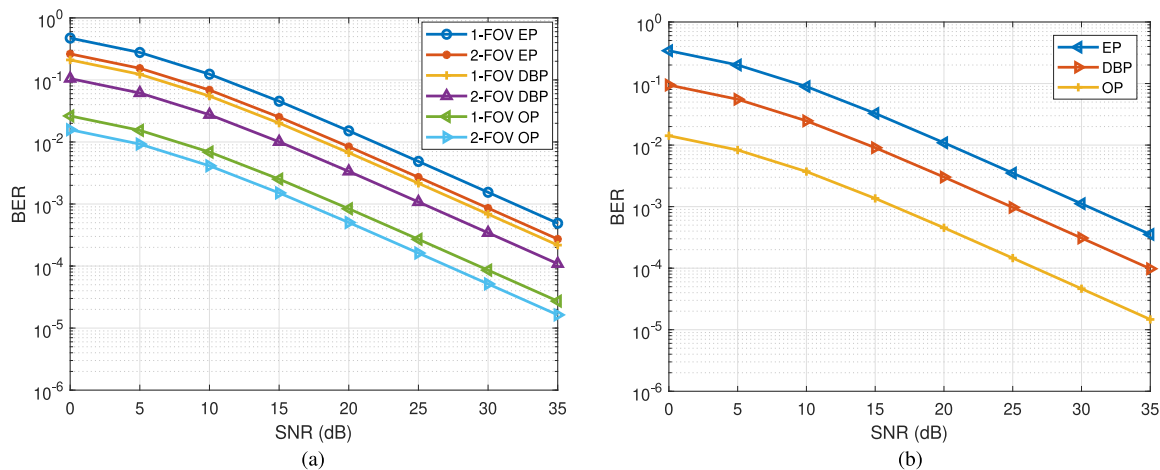


Fig. 12. BER performance of the MHCP with nonimaging and imaging receiver. (a) BER performance with nonimaging receiver. (b) BER performance with imaging receiver.

in the imaging receiver at the probability of 0.5, the received optical power for equal, distance-based, and OP allocation is 2.79, 3.38, and 4.01 dBm, respectively, as shown in Fig. 10(b). The MHCP with OP allocation performs better in both nonimaging receiver (1-FOV and 2-FOV) and imaging receiver configurations.

B. BER Performance

Fig. 11 shows the BER performance of the proposed system with EP and optimal allocation for nonimaging 1-FOV and 2-FOV receiver configuration, respectively. The derived BER expressions and the simulation results are in close agreement, which validates the mathematical derivations and justifies the approximations made in (29) and (34). It can also be observed in Fig. 11(a) that nonimaging 2-FOV receiver performs better than the 1-FOV receiver for EP allocation. For instance, to achieve the BER of 10^{-3} required SNR with 1-FOV receiver is 32 dB, while for 2-FOV receiver, the required SNR is 29 dB. Similarly, for OP allocation also, 2-FOV receiver is better as compared to 1-FOV receiver with required SNR of 17 and 19 dB, respectively, to achieve the BER of 10^{-3} as shown in Fig. 11(b).

Fig. 12 shows the BER performance for the proposed MHCP configuration with the nonimaging receiver and imaging receiver for equal, distance-based, and OP allocation. It can be observed that OP allocation gives better BER performance for both receiver configuration. For instance, 2-FOV receiver with equal and DBP to achieve the BER of 10^{-3} , the required SNR is 29 and 25 dB, respectively, whereas OP allocation for the same BER the required SNR is 19 dB as shown in Fig. 12(a). Fig. 12(b) compares the BER performance for imaging receiver with equal, distance-based, and OP allocation. It is evident that with the imaging receiver, optimal power allocation outperforms EP and DBP allocation for the proposed MHCP configuration. For instance, to achieve BER of 10^{-3} with imaging receiver in EP and DBP allocation strategy, the desired SNR is 31 and 25 dB, respectively, whereas with optimal power allocation strategy, the required SNR is only 17 dB.

VI. CONCLUSION

In this article, a random deployment of LEDs using the MHCP for an indoor VLC system with nonimaging receiver and imaging receiver structures is proposed. It has been shown that MHCP results in more uniform SNR in the room as compared to conventional LED deployments. The results of SNR at the receiver were compared for three different power allocation strategies namely, EP allocation, DBP allocation, and OP allocation. The proposed OP allocation is shown to provide more uniform SNR across the room with increased average SNR as well as the minimum variance between the two receiver locations inside the room. It has also been shown that the OP allocation performs better with the imaging receiver. The closed-form expression with MHCP is derived for the power allocation schemes with 1-FOV and 2-FOV receiver structure. The analytical results are in close agreement with the simulation results, which validates the analytical framework proposed in this article.

Furthermore, the results also demonstrate that MHCP with 2-FOV receiver and imaging receiver outperforms the nonimaging 1-FOV receiver with the proposed power allocation strategy. It has also been shown that the BER performance for optimal power allocation with nonimaging (2-FOV) and imaging receiver is better than equal and DBP allocation strategy.

REFERENCES

- [1] A. Khreishah, S. Shao, A. Gharaibeh, M. Ayyash, H. Elgala, and N. Ansari, "A hybrid RF-VLC system for energy efficient wireless access," *IEEE Trans. Green Commun. Netw.*, vol. 2, no. 4, pp. 932–944, Dec. 2018.
- [2] P. H. Pathak, X. Feng, P. Hu, and P. Mohapatra, "Visible light communication, networking, and sensing: A survey, potential and challenges," *IEEE Commun. Surv. Tut.*, vol. 17, no. 4, pp. 2047–2077, Oct.–Dec. 2015.
- [3] J. Grubor, S. Randel, K. Langer, and J. W. Walewski, "Broadband information broadcasting using LED-based interior lighting," *IEEE/OSA J. Lightw. Techn.*, vol. 26, no. 24, pp. 3883–3892, Dec. 2008.
- [4] B. Glushko, D. Kin, and A. Shar, "High bandwidth optical wireless network for gigabit communication," in *Proc. IEEE Global High Tech. Congr Electron.*, 2013, pp. 114–120.
- [5] Z. Chen, D. Tsonev, and H. Haas, "Improving SINR in indoor cellular visible light communication networks," in *Proc. IEEE Int. Conf. Commun.*, 2014, pp. 3383–3388.

- [6] A. Nuwanpriya, S. Ho, and C. S. Chen, "Indoor MIMO visible light communications: Novel angle diversity receivers for mobile users," *IEEE J. Sel. Areas Commun.*, vol. 33, no. 9, pp. 1780–1792, Sep. 2015.
- [7] C. He, T. Q. Wang, and J. Armstrong, "Performance of optical receivers using photodetectors with different fields of view in a MIMO ACO-OFDM system," *IEEE/OSA J. Lightw. Technol.*, vol. 33, no. 23, pp. 4957–4967, Dec. 2015.
- [8] P. Lei, Q. Wang, and H. Zou, "Designing LED array for uniform illumination based on local search algorithm," *J. Eur. Opt. Society-Rapid Publications*, vol. 9, pp. 1–6, 2014.
- [9] Z. Wang, W.-D. Zhong, C. Yu, and J. Chen, "A novel LED arrangement to reduce SNR fluctuation for multi-user in visible light communication systems," in *Proc. IEEE 8th Int. Conf. Inf., Commun. Signal Process.*, 2011, pp. 1–4.
- [10] I. Stefan and H. Haas, "Analysis of optimal placement of LED arrays for visible light communication," in *Proc. IEEE 77th Veh. Techn. Conf.*, Jun. 2013, pp. 1–5.
- [11] S. Pal, "Optimization of LED array for uniform illumination over a target plane by evolutionary programming," *Appl. Opt.*, vol. 54, no. 27, pp. 8221–8227, 2015.
- [12] A. Singh, A. Srivastava, V. A. Bohara, and G. S. V. Rao, "Performance of hybrid cellular-VLC link for indoor environments under dynamic user movement," *Phys. Commun.*, vol. 36, 2019, Art. no. 100816.
- [13] R. Guan, J.-Y. Wang, Y.-P. Wen, J.-B. Wang, and M. Chen, "PSO-based LED deployment optimization for visible light communications," in *Proc. IEEE Int. Conf. Wireless Commun. Signal Process.*, 2013, pp. 1–6.
- [14] M. T. Niaz, F. Imdad, S. Kim, and H. S. Kim, "Deployment methods of visible light communication lights for energy efficient buildings," *Opt. Eng.*, vol. 55, no. 10, 2016, Art. no. 106113.
- [15] S. Pergoloni, M. Biagi, S. Colonnese, R. Cusani, and G. Scarano, "Optimized LEDs footprinting for indoor visible light communication networks," *IEEE Photon. Techn. Lett.*, vol. 28, no. 4, pp. 532–535, Feb. 2016.
- [16] Y. Liu, Y. Peng, Y. Liu, and K. Long, "Optimization of receiving power distribution using genetic algorithm for visible light communication," *Proc. SPIE*, vol. 9679, 2015, Art. no. 96790I.
- [17] B. Matérn, *Spatial Variation*, vol. 36. Berlin, Germany: Springer, 2013.
- [18] A. Al-Hourani, R. J. Evans, and S. Kandeepan, "Nearest neighbor distance distribution in hard-core point processes," *IEEE Commun. Lett.*, vol. 20, no. 9, pp. 1872–1875, Sep. 2016.
- [19] J. Teichmann, F. Ballani, and K. G. van den Boogaart, "Generalizations of matérn's hard-core point processes," *Spatial Statist.*, vol. 3, pp. 33–53, 2013.
- [20] J. M. Kahn, R. You, P. Djahani, A. G. Weisbin, B. K. Teik, and A. Tang, "Imaging diversity receivers for high-speed infrared wireless communication," *IEEE Commun. Mag.*, vol. 36, no. 12, pp. 88–94, Dec. 1998.
- [21] H. Lu and Z. Su, "An indoor visible light communication model under the condition of multipath transmission," in *Proc. 8th Int. Conf. Image Sig. Process.*, 2015, pp. 1137–1141.
- [22] J. M. Kahn and J. R. Barry, "Wireless infrared communications," *Proc. IEEE*, vol. 85, no. 2, pp. 265–298, Feb. 1997.
- [23] W. H. Press, S. A. Teukolsky, W. T. Vetterling, and B. P. Flannery, *Numerical Recipes 3rd Edition: The Art of Scientific Computing*, 3rd ed. Cambridge, U.K.: Cambridge Univ. Press, 2007.
- [24] S. Rajagopal, R. D. Roberts, and S.-K. Lim, "IEEE 802.15. 7 visible light communication: Modulation schemes and dimming support," *IEEE Commun. Mag.*, vol. 50, no. 3, pp. 72–82, Mar. 2012.
- [25] I. Neokosmidis, T. Kamalakis, J. W. Walewski, B. Inan, and T. Spicopoulos, "Impact of nonlinear LED transfer function on discrete multitone modulation: Analytical approach," *IEEE/OSA J. Lightw. Technol.*, vol. 27, no. 22, pp. 4970–4978, Nov. 2009.
- [26] Y. Jiang, M. K. Varanasi, and J. Li, "Performance analysis of ZF and MMSE equalizers for MIMO systems: An in-depth study of the high SNR regime," *IEEE Tran. Inf. Theory*, vol. 57, no. 4, pp. 2008–2026, Apr. 2011.
- [27] Z. Ghassemlooy, W. Popoola, and S. Rajbhandari, *Optical Wireless Communications: System and Channel Modelling With MATLAB*. Boca Raton, FL, USA: CRC Press, 2017.
- [28] T.-C. Bui, S. Kiravittaya, K. Sripimanwat, and N.-H. Nguyen, "A comprehensive lighting configuration for efficient indoor visible light communication networks," *Int. J. Opt.*, vol. 2016, 2016, Art. no. 8969514.
- [29] I. Din and H. Kim, "Energy-efficient brightness control and data transmission for visible light communication," *IEEE Photon. Techn. Lett.*, vol. 26, no. 8, pp. 781–784, Apr. 2014.
- [30] L. Zeng *et al.*, "High data rate multiple input multiple output (MIMO) optical wireless communications using white LED lighting," *IEEE J. Sel. Areas Commun.*, vol. 27, no. 9, pp. 1654–1662, Dec. 2009.